International Journal of Fluid Machinery and Systems
Vol. 1, No. 1. October-December 2008

Original Paper

Choked Surge in a Cavitating Turbopump Inducer

Toshifumi Watanabe[1], Donghyuk Kang[1], Angelo Cervone[1], Yutaka Kawata[2]

Yoshinobu Tsujimoto[1]

[1]Graduate School of Engineering Science, Osaka University
1-3 Machikaneyama, 560-8531, Toyonaka, Osaka, Japan
[2]Department of Mechanical Engineering, Osaka Institute of Technology
5-16-1, Omiya, Asahi-Ku, 535-8505, Osaka, Japan

Abstract

During an experimental investigation on a 3-bladed and a 4-bladed axial inducer, a severe surge instability was observed in a range of cavitation number where the blade passage is choked and the inducer head is decreased from non-cavitating value. The surge was stronger for the 4-bladed inducer as compared with a 3-bladed inducer with the same inlet and outlet blade angles. For the 4-bladed inducer, the head decreases suddenly as the cavitation number is decreased. The surge was observed after the sudden drop of head. This head drop was found to be associated with a rapid extension of tip cavity into the blade passage. The cause of surge is attributed to the decrease of the negative slope of the head-flow rate performance curve due to choke. Assuming that the difference between the 3 and 4-bladed inducers is caused by the difference of the blockage effects of the blade, a test was carried out by thickening the blades of the 3-bladed inducer. However, opposite to the expectations, the head drop became smoother and the instability disappeared on the thickened blade inducer. Examination of the pressure distribution on both inducers could not explain the difference. It was pointed out that two-dimensional cavitating flow analyses predict smaller breakdown cavitation number at higher flow rates, if the incidence angle is smaller than half of the blade angle. This causes the positive slope of the performance curve and suggests that the choked surge as observed in the present study might occur in more general cases.

Keywords: Cavitation, instabilities, inducers, surge.

1. Introduction

Most cavitation instabilities such as cavitation surge and rotating cavitation occur in the range where head is not yet decreased due to cavitation and are caused by a positive value of the mass flow gain factor (Tsujimoto et al. [1]). Young [2] has shown that a positive value of the pressure gain factor, defined as the slope of the suction performance curve (in which the head coefficient is expressed as a function of the cavitation number), has a stabilizing effect. Usually, all cavitation instabilities cease, and stable operation can be realized, once the cavity extends into the blade passage and the head starts to decrease (head breakdown).

However, severe shaft vibrations were observed under head breakdown conditions in a liquid hydrogen turbopump inducer during the development of the LE-7A engine for the H-IIA rocket (Shimura et al. [3]). Figure 1 shows the suction performance of the LE7-A liquid hydrogen turbopump inducer and the amplitude of shaft vibrations for two groups of flow rates $Q/Q_d \approx 0.98$ and $Q/Q_d \approx 0.95$. For $Q/Q_d \approx 0.95$, the amplitude becomes larger at the cavitation number value for which the inducer head rapidly drops. The head is kept nearly constant above and below the breakdown cavitation number. For $Q/Q_d \approx 0.98$, the head smoothly decreases and the intensity of shaft vibrations (not shown in the Figure) do not increase. The sudden head drop for $Q/Q_d \approx 0.95$ is not caused by the instability since the head drop is not recovered at the smaller cavitation number where the vibrations amplitude gets smaller again. For the cavitation number σ_{high}, higher than the breakdown cavitation number, the head is larger for the smaller flow rate and the performance curve (head as a function of the flow rate) has a negative slope. On the other hand, for the cavitation number σ_{low} (lower than breakdown), the head is smaller for smaller flow rates and the performance curve has a positive slope. These situations are sketched in Fig.2.

For compressors and fans, it is well known that the positive slope of the performance curve can cause flow instabilities like surge and rotating stall. It was experimentally found (Shimura et al. [3]) that the shaft vibrations of the liquid hydrogen inducer for

Received 22 May 2008; revised 22 July 2008; accepted for publication 17 August 2008.
Corresponding author: Yoshinobu Tsujimoto yoshi@me.es.osaka-u.ac.jp

the LE-7A engine were caused by a pressure pattern rotating around the impeller with an angular velocity about 50% of the impeller rotation. Since the head breakdown is caused by choke, this phenomenon can be called “rotating choke”. Semenov et al. [4] made a two dimensional stability analysis of the cavitating flow through a cascade by means of a waked cavity model, showing that the rotating choke can actually occur under choked conditions. However, the sudden drop of inducer head is unusual and has not been explained yet. More recently, Uchiumi and Kamijo [5] presented the results of an experimental investigation on several 3-bladed inducers, confirming that rotating choke can be observed in presence of sudden head drop.

The present paper treats a severe surge recently observed under choked conditions in a 4-bladed inducer. The suction performance curves of the tested inducers exhibit a sudden drop which is quite similar to that shown in Fig. 1. So, this can be considered as another instability mode, the “choked surge”, caused by the positive slope of the performance curve due to choke.

The purpose of the present study is to report about this newly found instability and to discuss about its causes as well as the factors by which it is affected.

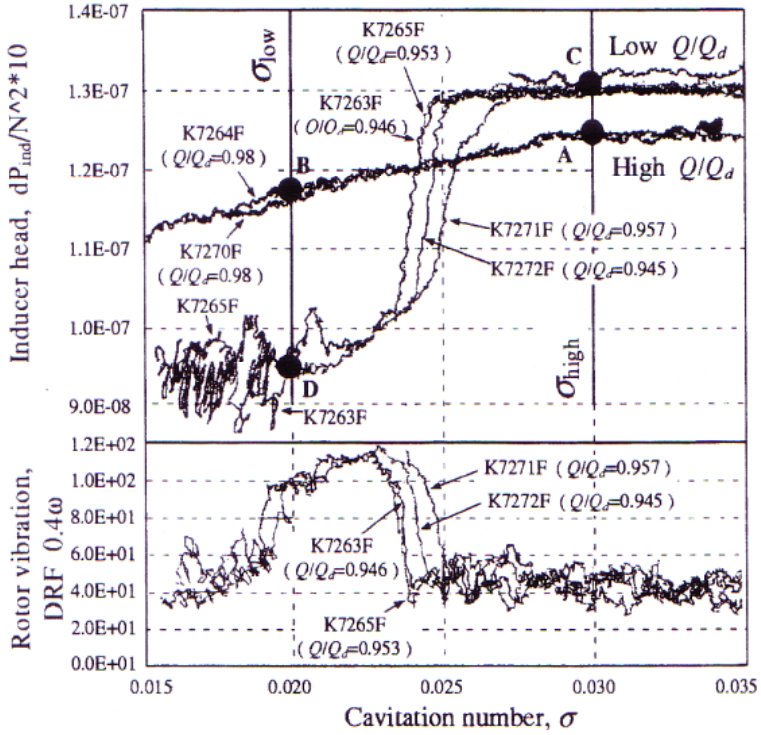

Fig. 1 Suction performance of the LE-7A liquid hydrogen turbopump (top).
Amplitude of the shaft vibrations for two groups of flow rates (bottom).

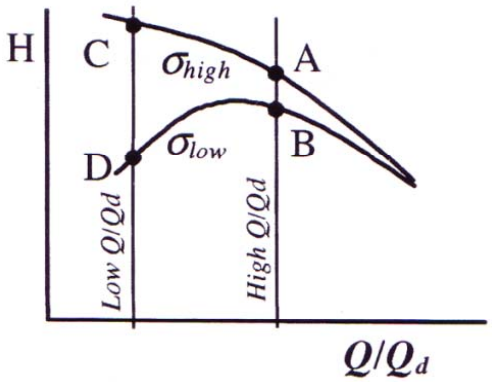

Fig. 2 Sketch of the head-flow rate curve at two different cavitation numbers.

2. Experimental Facility and Test Inducers

Figure 3 schematically shows the test facility used for the experiments. The cavitation number is adjusted by controlling the tank pressure with a vacuum pump and a relief valve. The water level in the tank is set to be 800 mm above the centerline of the inducer. In order to attain a sufficiently small cavitation number, three perforated plates have been placed at the exit flange of the tank. The first plate had 69 circular holes with a diameter of 11 mm, the second had 60 holes with a diameter of 13 mm and the third had 69 holes with a diameter of 14 mm. The holes were equally distributed within the inlet pipe, which has an inner diameter of 203.3 mm. The use of multiple plates was intended to generate a smoother pressure drop and minimize the effect of cavitation on each plate. However, a certain amount of bubbles were flowing down the test section at smaller cavitation numbers.

Figure 4 shows the details of the test section around the inducer. The inlet static pressure p_1 is measured 312.5 mm upstream of the tip leading edge of the blades, and the outlet static pressure is measured 55.5 mm downstream of the tip leading edge. The

inlet pressure fluctuations are measured by flush mounted pressure transducers located 54.5 mm upstream of the tip leading edge.

Figure 5 shows the 4-bladed inducer used for the experiments. For comparison, a 3-bladed inducer with similar blade design was also tested. The principal dimensions of these inducers are shown in Table 1. The design flow coefficient, defined as the ratio of the mean axial velocity at the axial location of leading edge at hub (including hub blockage) to the tip speed, is $\phi_d = 0.078$ for both inducers. They both have a helical design with tip blade thickness of 2 mm. For this reason, the blockage effect of the blades is larger for the 4-bladed inducer. The noncavitating performance curves of these inducers, based on static pressures, are shown in Fig. 6. No significant difference can be observed between 3- and 4-bladed inducers. To increase the blockage effect of the blades, the thickness of the 3-bladed inducer blades was increased by pasting rubber sheets of thickness 1.2 mm on the pressure side, from the leading edge to the trailing edge of the next blade throughout the blade passage. After this modification, the pressure coefficient was somewhat decreased but the performance curve remained nearly parallel to the original one.

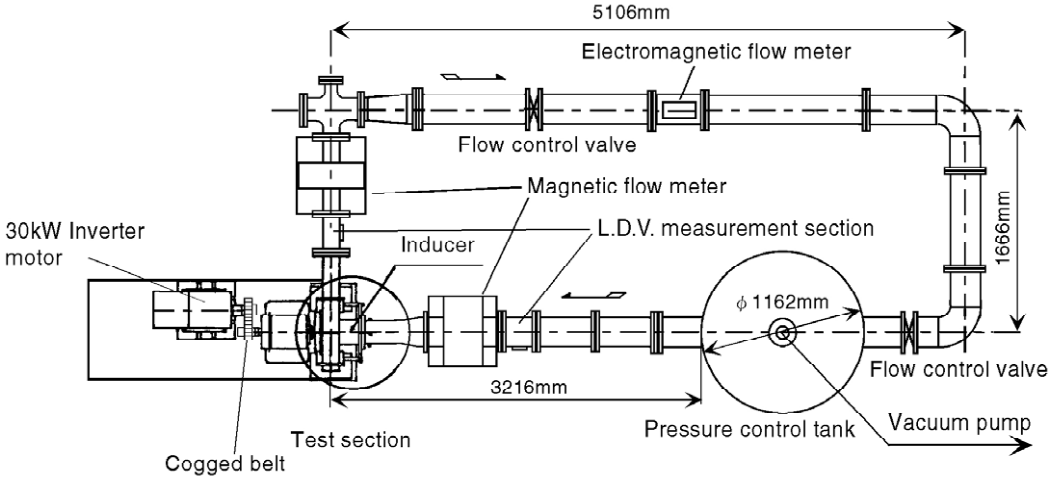

Fig. 3 Schematic drawing of the test facility.

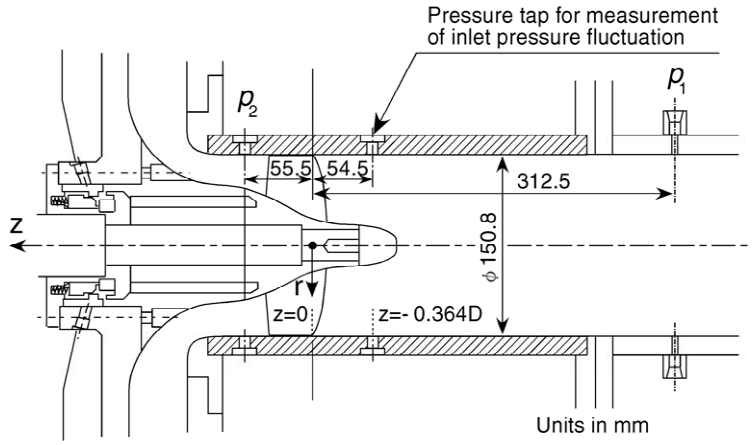

Fig. 4 Schematic drawing of the inducer test section, showing the position of the pressure transducers.

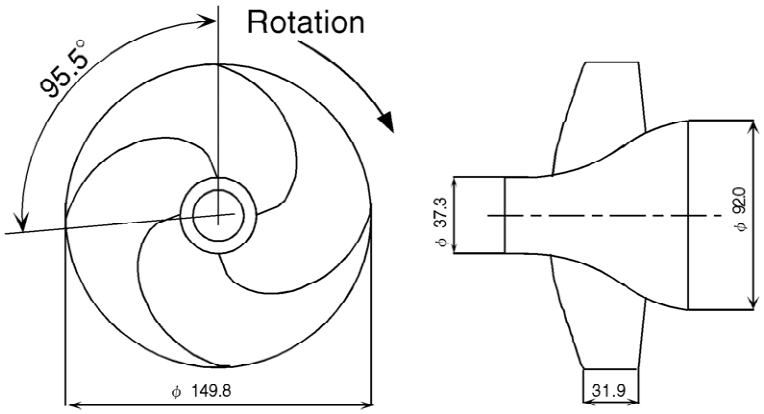

Fig. 5 The 4-bladed inducer used for the experiments.

Table 1 Geometrical properties of the 3-bladed and 4-bladed inducers used for the experiments.

Number of blades	3	4
Tip diameter	149.8 mm	149.8 mm
Inlet tip blade angle	7.5 deg	7.5 deg
Outlet tip blade angle	9.0 deg	9.0 deg
Hub/tip ratio at the inlet	0.25	0.25
Hub/tip ratio at the outlet	0.51	0.53
Solidity at tip	1.91	1.91
Design flow coefficient	0.078	0.078
Tip clearance	0.5 mm	0.5 mm
Blade thickness at tip	2 mm	2 mm

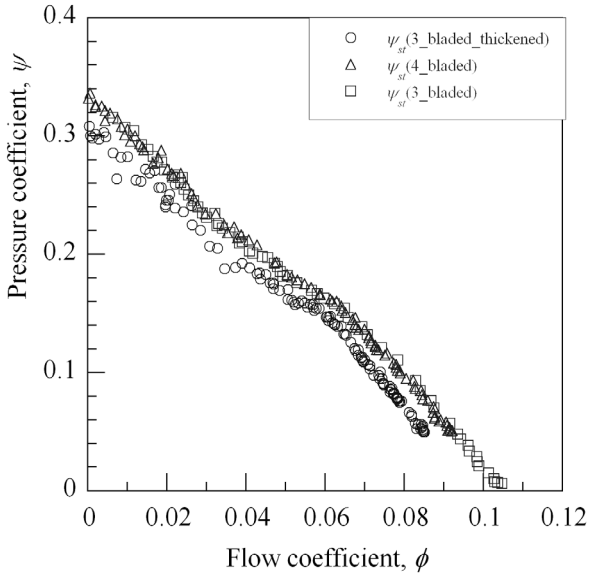

Fig. 6 Noncavitating performance curves for the 4-bladed, 3-bladed and 3-bladed thickened inducers.

3. Results for the 4-Bladed Inducer

Figure 7 shows the suction performance of the 4-bladed inducer at 3000 rpm. The flow rate is adjusted under noncavitating conditions using the flow control valve. The tank pressure is first lowered to its minimum value and then increased gradually while taking the data, keeping the same valve opening. The flow rate is somewhat decreased at smaller cavitation numbers due to the increase of valve resistance caused by cavitation. For the data presented in Fig. 7, the sampling rate was 200 sps (samples-per-second) and a 4-points average was made after averaging over 100 points, corresponding to averaging over 2 seconds. The data are largely scattered within $0.01 < \sigma < 0.02$ for flow rates below $\phi = 0.077$, although the fluctuations are only qualitative since the pressure was measured by a differential transducer through a long pipe. Plots based on a sampling rate of 1000 sps and averaging over 6000 points, corresponding to averaging over 6 seconds, are shown in Fig. 8. We observe sudden head drops for flow rates below $\phi = 0.077$. It is also important to note that the curves are shifted horizontally and we can find a region where the head is higher at higher flow rates. In this region a large scatter is found in Fig. 7. The amplitude of oscillations decreases when rotational speed is decreased.

The suction performance curve obtained at 2000 rpm, with a sampling rate of 200 sps and a 4-point average after averaging over 100 points (the same as for Fig. 7) is shown in Fig. 9. The theoretical breakdown cavitation number σ_B obtained applying the model by Brennen and Acosta [6], based on a two-dimensional linear analysis, is also shown in the Figure. The comparison is as good as one might expect considering the approximations in the theory. The scatter of the experimental data is smaller as compared with Fig. 7 for 3000 rpm. We can observe a sudden head drop at lower flow coefficients but it can not be observed a region where the head is higher for higher flow rates, except for $\phi = 0.077$ and $\phi = 0.078$. However, the space between the curves at different flow rates becomes smaller below the cavitation number for which the sudden head drop occurs. So, if inlet pressure or cavitation number fluctuate, a positive slope of the head-flow performance curve easily occurs after head breakdown. This is practically shown in Fig. 8.

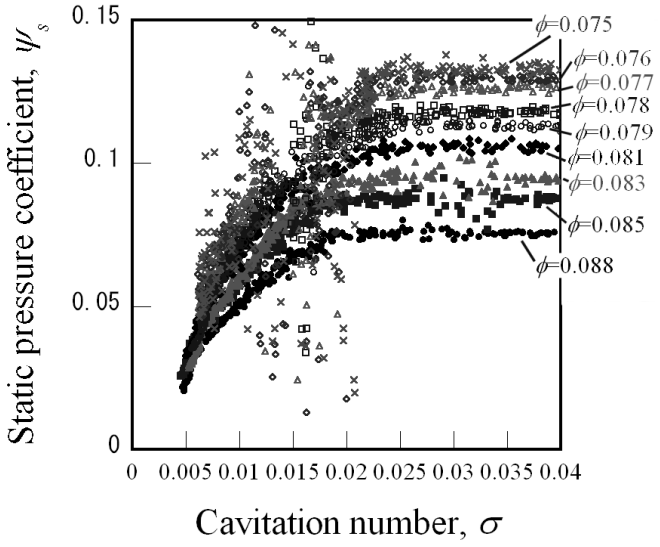

Fig. 7 Suction performance of the 4-bladed inducer at 3000 rpm.
The sampling rate is 200 sps and each point of the plot is obtained by 4-point average made after averaging over 100 samples.

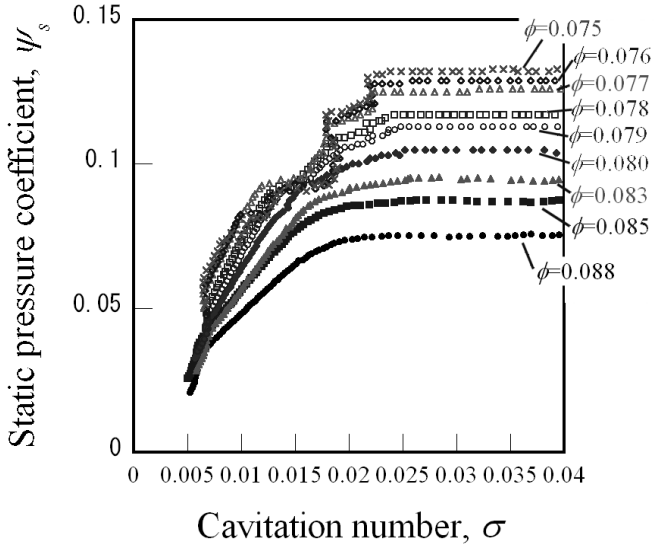

Fig. 8 Suction performance of the 4-bladed inducer at 3000 rpm.
The sampling rate is 1000 sps and each point of the plot is obtained by averaging over 6000 samples.

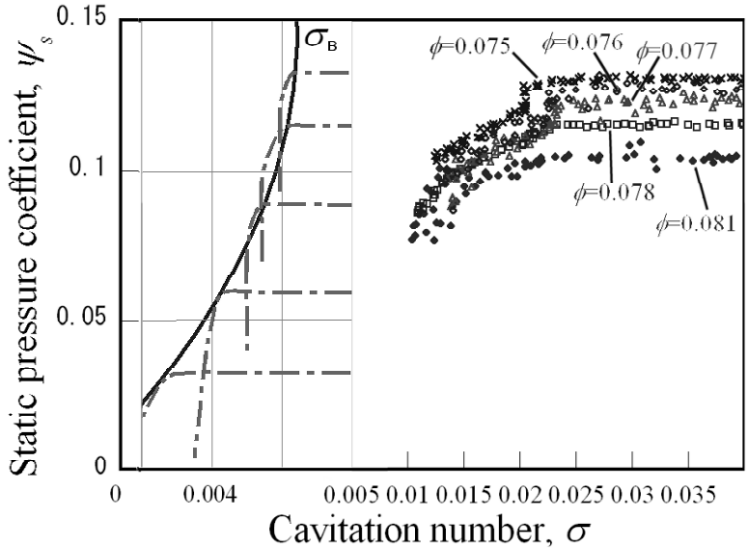

Fig. 9 Suction performance of the 4-bladed inducer at 2000 rpm; the sampling rate is 200 sps and each point of the plot is obtained by 4-point average made after averaging over 100 samples.
On the left hand side, breakdown cavitation number σ_B obtained by Brennen-Acosta simplified model is shown, with sketches of suction performance curves. For σ_B , the x-axis scale has been enlarged.

Figure 10 shows the spectrum of inlet pressure fluctuations at 3000 rpm, for several values of the flow coefficient. We observe a component in the frequency range 5-10Hz (10-20% of the rotational frequency) at a cavitation number $\sigma = 0.01$ 0.02 . The latter agrees with the region of large scatter in Fig. 7. The fluctuations have the same phase around the circumference, suggesting a surge mode oscillation. The peak is higher at smaller flow rates and disappears at higher flow coefficients. Near $\sigma = 0.04$ we observe a component at 50 Hz, caused by attached cavitation. The intensity of oscillations for the surge mode is much larger than the attached cavitation.

Figure 11 shows pictures from high speed video taken at the design flow coefficient $\phi = 0.078$ and 3000 rpm. At a higher cavitation number $\sigma = 0.020$, where the surge mode is about to occur, the cavitated region extends almost into the blade passage. At $\sigma = 0.007$, where the surge mode is no more observed, the cavity almost reaches the trailing edge. At $\sigma = 0.012$, where the surge mode is occurring, the cavity extends downstream of the trailing edge at a moment, as shown by the picture number 6. At this moment no backflow vortex cavitation can be found and the instantaneous flow rate would be higher. Eventually, a large number of backflow vortices appear at the inlet (picture no. 1) and grow up while increasing in volume and decreasing in number (pictures 1-3). Since it has been shown (Yokota et al. [7]) that only smaller number of backflow vortices can exist at smaller flow rates, the flow rate can be assumed to be decreasing during this period. At the same time, cavitation in the blade passage becomes shorter. Then, the backflow vortex cavities collapse and the cavitating region in the passage extends downstream and finally some part of them is shed from the inducer (pictures 4-6).

Since the pressure fluctuation has the same phase all around theinducer inlet and the inlet mass flow is oscillating as observed above, the instability observed here can be called “choked surge”, defined as a one-dimensional system instability with axial mass flow oscillations, caused by the positive slope of the performance curve due to choke generated by cavitation. Although the test facility includes two magnetic flow meters, the mass flow fluctuation could not be measured in the present case due to a technical problem.

The sudden drop of the suction performance and the surge mode have been observed on the 4-bladed inducer even without the

perforated plates (Yoshida et al. [8]). Furukawa et al. [9] observed a similar head drop and surge mode on a 2-bladed helical inducer with a tip blade angle of 11 degrees, a tip solidity of 2.0 and without leading edge sweep, at a very small flow coefficient $\phi = 0.017$. However, the origin of the instability was not discussed in the paper.

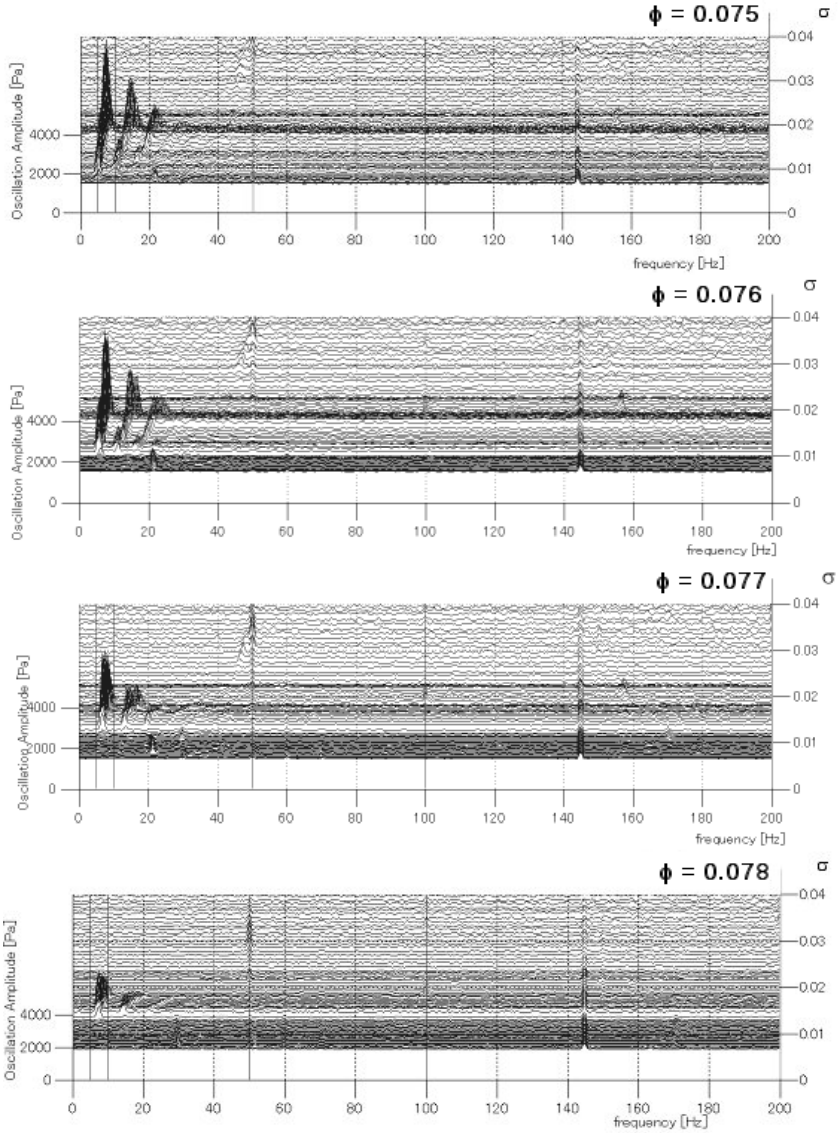

Fig. 10 Waterfall plots of the pressure fluctuations at the inlet of the 4-bladed inducer, at various flow coefficients and a rotating speed of 3000 rpm.

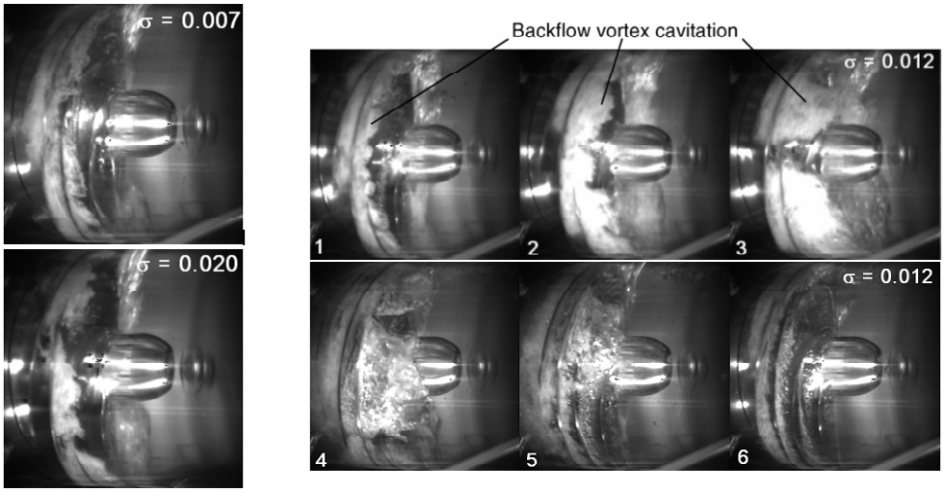

Fig. 11 Pictures of the 4-bladed inducer from high speed video, taken at the design flow coefficient $\phi = 0.078$ and a rotating speed of 3000 rpm. Pictures for cavitation numbers 0.020 and 0.007 (left); series of successive pictures for cavitation number 0.012, corresponding to one cycle of oscillation (right).

4. Results for the 3-Bladed Inducer

Figure 12 shows the suction performance of the 3-bladed inducer at 3000 rpm, obtained with a sampling rate of 200 sps and a

4-points average after averaging over 100 points (same as Figs. 7 and 9). If we compare the curves with Fig. 7 for the 4-bladed inducer, the scatter between $\sigma = 0.010$ and $\sigma = 0.015$ is smaller. Figure 13 shows the results based on a sampling rate of 1000 sps and averaging over 6000 points. We can find a region where the head is higher at higher flow rates but the difference of the head is smaller as compared with Fig. 8 for the 4-bladed inducer. Figure 14 shows the suction performance obtained at 2000 rpm where no surge mode oscillations occur. The data show larger scatter as compared with Fig. 9 for the 4-bladed inducer, but the head decreases gradually and there is no sudden head drop.

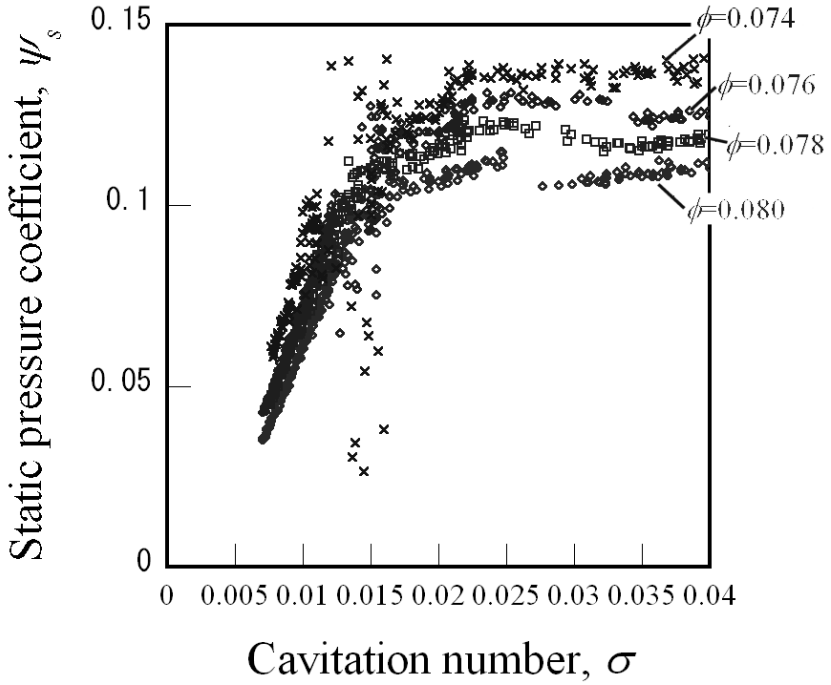

Fig. 12 Suction performance of the 3-bladed inducer at 3000 rpm. The sampling rate is 200 sps and each point of the plot is obtained by 4-points average made after averaging over 100 samples.

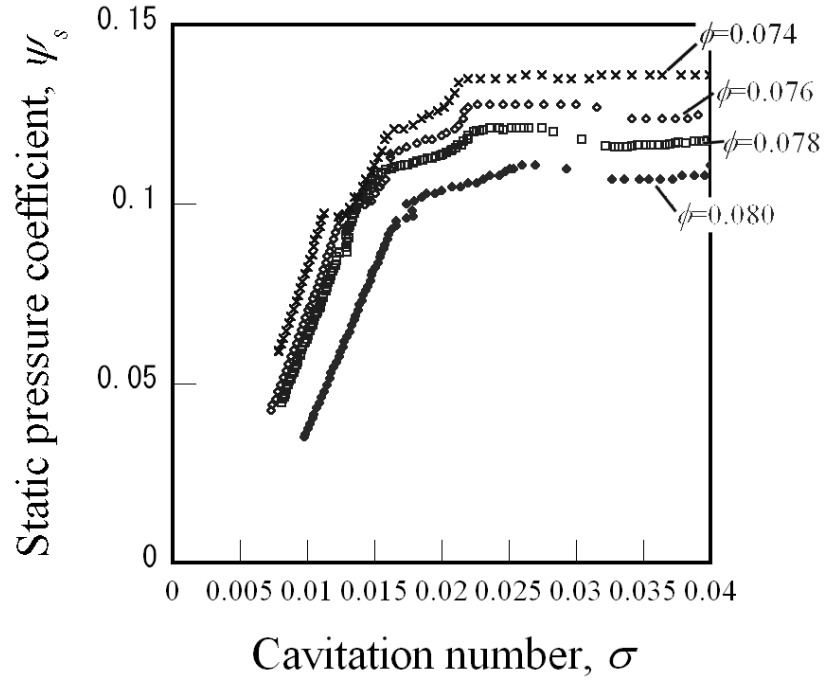

Fig. 13 Suction performance of the 3-bladed inducer at 3000 rpm. The sampling rate is 1000 sps and each point of the plot is obtained by averaging over 6000 samples.

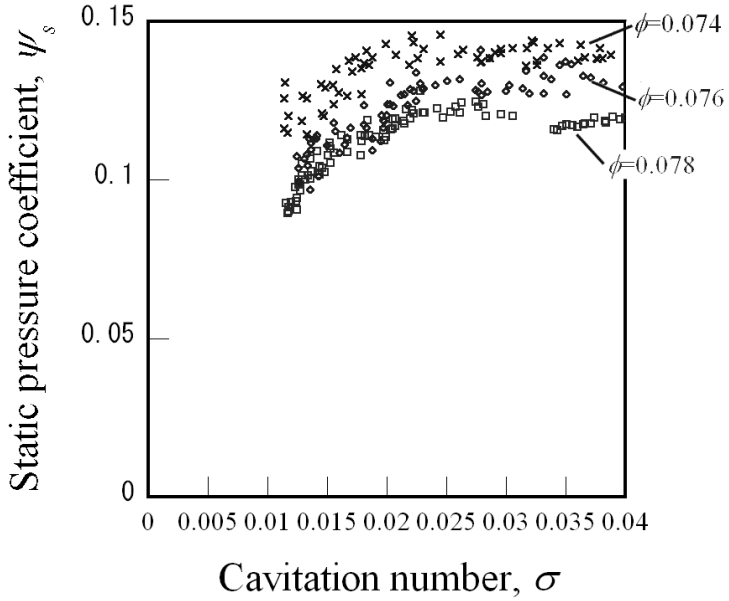

Fig. 14 Suction performance of the 3-bladed inducer at 2000 rpm. The sampling rate is 200 sps and each point of the plot is obtained by 4-points average made after averaging over 100 samples.

Figure 15 shows the spectrum of inlet pressure fluctuations at 3000rpm. We observe a component at a frequency of 5-10 Hz. This component is a surge mode oscillation and occurs in the range $\sigma = 0.012 \sim 0.016$, corresponding to the larger scatter in Fig. 12. However, the amplitude of oscillations is smaller as compared with the 4-bladed inducer data shown in Fig. 10. At $\phi = 0.074$, we have a component around 30 Hz within the range $\sigma = 0.015 \sim 0.02$. The mode of oscillation could not be identified from the phase difference of the pressure fluctuations at different circumferential locations but may be the cause of the dip in the suction performance curve around $\sigma = 0.015 \sim 0.02$. The component at 40-50 Hz was identified to be a one-cell mode, rotating in the same direction of the impeller at 80-100% of the impeller speed. At higher cavitation numbers, this mode switches to an attached cavitation at a frequency of 50 Hz. When the attached cavitation occurs, the head is somewhat decreased in the suction performance curve shown in Fig. 12. On the other hand, the surge mode at lower frequency causes larger scatter. This may be caused by a slower response of the pressure measurement system.

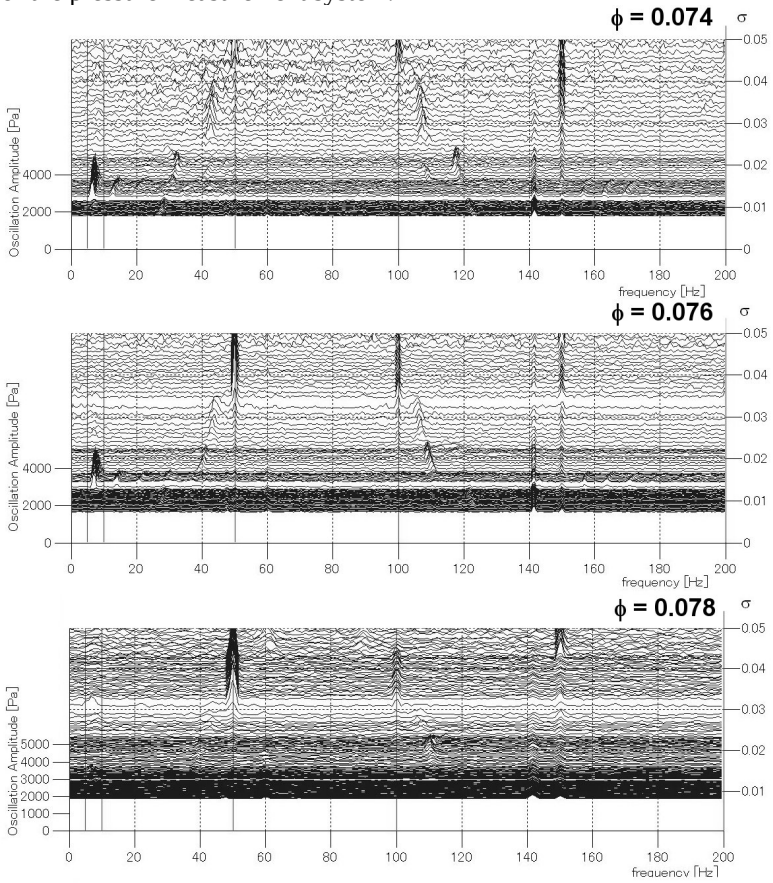

Fig. 15 Waterfall plots of the pressure fluctuations at the inlet of the 3-bladed inducer, at various flow coefficients and a rotating speed of 3000 rpm.

5. Discussion

5.1 Blockage effect of blades

To understand the difference between the 3- and 4-bladed inducers, the thickness of the 3-bladed inducer blades (originally 2 mm) was increased by pasting rubber sheets of thickness 1.2 mm on the pressure side, from the leading edge to the trailing edge of the adjacent blade, expecting that the drop of the performance curve (as shown in Figs. 8 and 9) and severe choked surge (as shown in Fig. 10) occur by thickening the blades. Figures 16 and 17 show the suction performance and the inlet pressure spectrum at flow coefficients $\phi = 0.074$ and $\phi = 0.078$ and 3000 rpm. If we compare the suction performance in Fig. 16 for thickened inducer (the sampling rate is 200 sps and 4-points average was made after averaging over 100 points) to Fig. 12 for unthickened case, we find that the scatter around $\phi = 0.010 \sim 0.017$, observed in the unthickened inducer, disappeared in the thickened case. The suction performance curve is smoother as compared with Fig. 13 and no sudden drop as shown in Figs. 8 and 9 for the 4-bladed inducer was found. If we compare the spectrum in Fig. 17 for thickened inducer to Fig. 15 for unthickened case, we observe that the choked surge around $\sigma = 0.010 \sim 0.017$, observed in the unthickened inducer, disappears in the thickened one, although a surge component appears around $\sigma = 0.03 \sim 0.04$. Thus, the blockage effects are opposite to our expectations and the difference between the results on the 3-bladed and 4-bladed inducers cannot be attributed to the blockage effects.

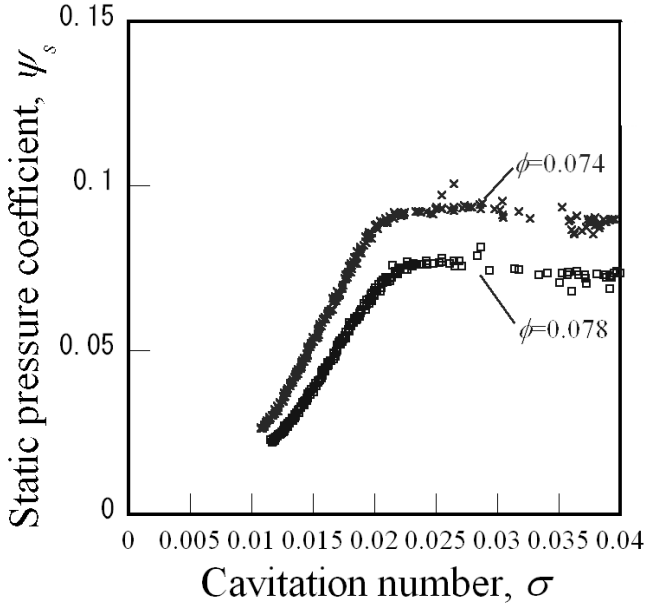

Fig. 16 Suction performance of the 3-bladed thickened inducer at 3000 rpm. The sampling rate is 200 sps and each point of the plot is obtained by 4-points average made after averaging over 100 samples.

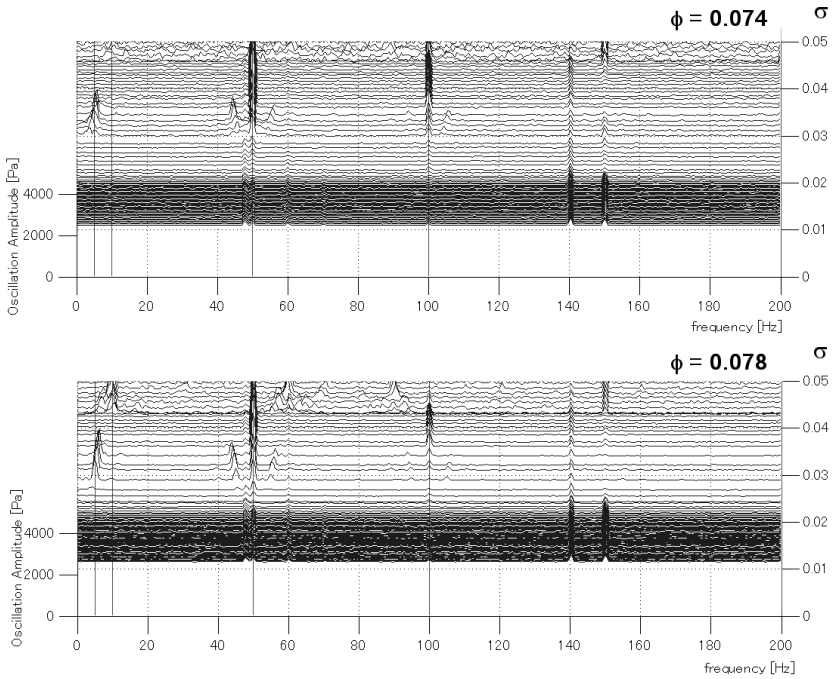

Fig. 17 Waterfall plots of the pressure fluctuations at the inlet of the 3-bladed thickened inducer, at flow coefficients $\phi = 0.074$ (top) and $\phi = 0.078$ (bottom) and a rotating speed of 3000 rpm.

5.2 Effects of Perforated Plates

As already mentioned, in the 4-bladed inducer, the sudden drop of suction performance and the surge mode instability also occur without the perforated plates in the suction line. For the 3-bladed inducer, the cavitation number could not be decreased to

the head breakdown with the present configuration of the facility. To determine the effects of the perforated plates, experiments were carried out by using one plate with 69 holes of 12 mm diameter. Figure 18 compares the spectrum at $\phi = 0.076$ for the 3- and 4-bladed unthickened inducers, at 3000 rpm with the single perforated plate. By comparing with Figs. 10 and 15, we find that the amplitude of the surge is significantly decreased with the single perforated plate. Specifically, the amplitude becomes negligible in the case of the 3-bladed inducer. With the single plate, the total resistance is smaller but more severe cavitation is expected on the plate. The cavitation downstream of a plate will have an effect to prevent the downstream disturbance to be transmitted upstream. This will decrease the damping effect of the resistance of the perforated plate on downstream disturbance. So, we cannot explain why the amplitude is decreased but the results show that the cavitation at the perforated plate is not causing the surge.

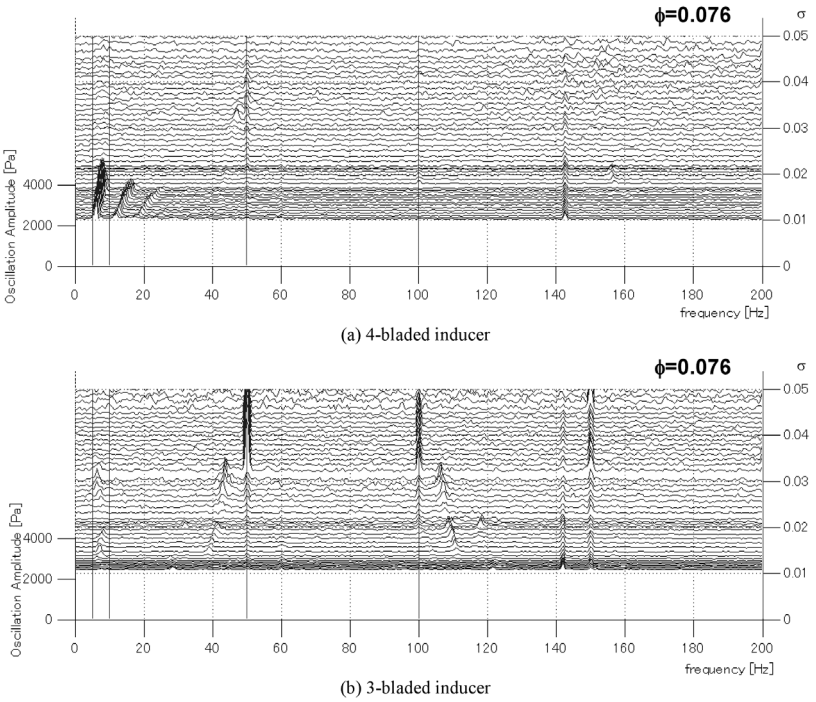

Fig. 18 Spectrum of inlet pressure fluctuations, with single orifice plate, at $\phi = 0.076$ and 3000 rpm.

5.3 Development of Cavity

In order to investigate the correlation between cavity development and head breakdown, the location of the closure point of the tip cavity was determined from pictures. Since the cavity is fluctuating, the location was determined as an average of four pictures under the same flow conditions. Figure 19 shows the location of the cavity closure point and the pressure coefficient for $\phi = 0.074$, in the 3-bladed and 4-bladed inducers.

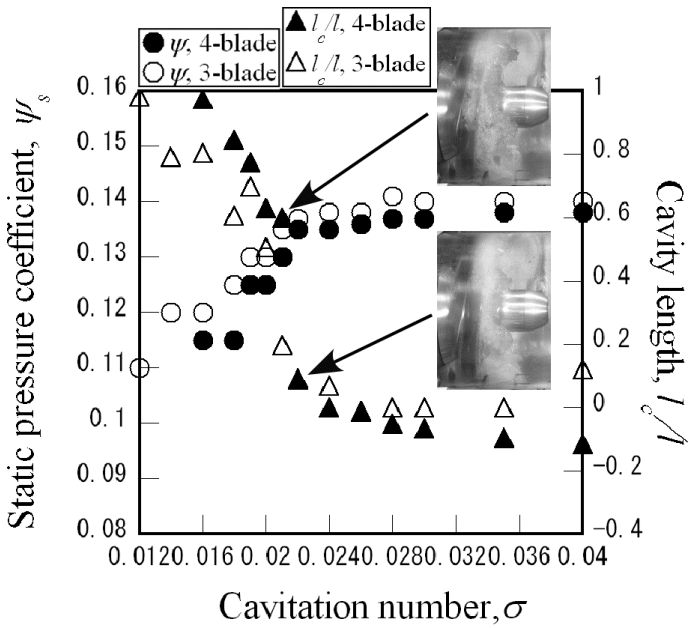

Fig. 19 Cavity length and pressure coefficient of the 3-bladed and 4-bladed inducers, as functions of σ, for $\phi = 0.074$.

For this series of tests, the head drop is not so "sudden" as compared with Fig. 9, since the cavitation number was increased very slowly during the experiments. The location with $l_c / l = 0$ corresponds to the leading edge of the next blade (entrance to the blade passage) and $l_c / l = 1$ corresponds to the trailing edge of the blade to which the cavity is attached (exit of the blade passage). It can be found that:

1) The head starts to decrease when the cavity extends into the blade passage;

2) In the 4-bladed inducer the cavity develops rapidly once it gets into the blade passage, but the development is rather smooth for the 3-bladed inducer. Two typical pictures of cavitation are shown in the Figure. At $\sigma = 0.022$ the cavity trailing edge is almost at the leading edge of the next blade, but it extends to the trailing edge at $\sigma = 0.021$.

It is therefore proved that the sudden decrease in head for the 4-bladed inducer is caused by the rapid development of the cavity. However, the reasons of this development are not fully understood yet. It was found that the 3-bladed inducer has larger backflow under noncavitating conditions as compared with the 4-bladed inducer, and the backflow becomes smaller near the breakdown. For the 4-bladed inducer, the backflow extent does not change as much as in the case of the 3-bladed inducer.

5.4 Pressure Distribution

With the hope of explaining the rapid development of the cavity in the 4-bladed inducer, the pressure distributions on the 3- and 4-bladed inducer blades were calculated by using a commercial code under noncavitating steady condition. However, no significant difference could be observed although the pressure is slightly lower for the 4-bladed inducer due to the larger blockage effect of the blades.

5.5 Breakdown Cavitation Number

By a free-streamline analysis of the cavitating flow through a semi-infinite cascade, Brennen and Acosta [6] have shown that the breakdown cavitation number σ_B can be approximated by $\sigma_B \approx \alpha(\beta - \alpha) + \beta^2 d$, where α is the incidence angle, β is the blade angle and d is the ratio of the blade thickness to the distance between blades measured normal to the blades (see also Brennen [10]). By applying the above equation, it can be found that the breakdown cavitation number becomes maximum at $\alpha = \beta / 2$, which corresponds to the flow coefficient $\phi = 0.0655$ for the present case, and the maximum cavitation number is 0.0046 for the 4-bladed inducer, if we use the tip incidence angle α evaluated by assuming uniform axial velocity distribution. On the left hand side of Fig. 9, the breakdown cavitation number σ_B obtained by Brennen-Acosta model and several schematic suction performance curves are shown by evaluating the flow coefficient and hence the incidence angle α at each head coefficient from the measured performance curve. We can find that the breakdown cavitation number becomes smaller for larger flow rates, if the flow coefficient is larger than $\phi = 0.0655$. For these cases the head after breakdown can become larger for larger flow rate and this can cause instabilities after breakdown. This result suggests that instabilities may occur generally for the cases with incidence angle smaller than half of the blade angle. However, the authors are aware that no report of such instabilities have be presented so far, except for Refs. [3]-[5] and the present paper. The authors are not sure if three dimensional flow effects really have a suppressing role as discussed above, or the tests under breakdown conditions are limited since it is beyond the range of normal operation.

6. Conclusions

A newly found cavitation instability, the “choked surge”, has been reported in the present paper. This instability occurs in the region of cavitation number where the head is decreased due to cavitation were discussed. For the 4-bladed inducer, the surge can be correlated with a sudden drop in suction performance. Under surge, the average suction performance suggests positive slope of static pressure rise-flow coefficient performance curve. However, under the conditions in which the surge is suppressed, the slope is still negative although it becomes smaller under choked condition. Since the distance between the suction performance curves at different flow rates becomes smaller and the slope of the suction performance curve is steeper under breakdown conditions, the slope of the head-flow curve may become positive associated with the fluctuation in cavitation number.

Thus, considering that the positive slope of the performance curve is not as evident as in the case of “rotating choke”, the authors believe that “choked surge” is a one-dimensional system instability with axial mass flow fluctuation at the inlet, mainly associated to the decreased negative slope of the performance curve.

Various factors affecting the occurrence of “choked surge” were examined. Stronger fluctuations occur in the 4-bladed inducer as compared to a 3-bladed inducer with the same design except for blade thickness. In order to simulate higher blockage effects of the blades as in the 4-bladed inducer, the blade thickness of the 3-bladed inducer was increased. However, contrarily to the expectations, no surge occurred in the thickened 3-bladed inducer. The effects of perforated plates upstream and pressure distribution on the blade were also examined. After all these efforts, the only definite finding was that the “choked surge” is closely related to the inducer performance curve after breakdown.

Recently, the authors have learned about a severe surge in a double suction industrial pump which typically occurs in the regions where the breakdown cavitation number is smaller for larger flow rate, as shown on the right hand side of Fig. 9. This may also be associated with the decrease of negative slope of the performance curve, although detailed examinations have not been made yet.

However, further investigations (both experimental and analytical) are needed in order to fully understand the origins and characteristics of the “choked surge” instability.

Acknowledgments

The authors would like to express their sincere gratitude to Professors Allan J. Acosta and Christopher E. Brennen of California Institute of Technology and Mr. Patrick Arellano of Pratt&Whitney Rocketdyne for their fruitful discussions and useful suggestions. This work has been supported by the Ministry of Education, Science, Sports and Culture through the Grant-in-Aid for Scientific Research. Dr. Cervone would also like to acknowledge Japan Society for the Promotion of Science (JSPS), which funded his post-doc research fellowship at Osaka University.

Nomenclature

d	Ratio of blade thickness to normal distance between the blades [-]	α	Inlet incidence angle at blade tip [rad]
l	Blade chord at tip [m]	β, β_1	Inlet tip blade angle [rad]
l_c	Cavity length [m]	ϕ	Flow coefficient [-]
p_1	Inlet static pressure [Pa]	ϕ_d	Design flow coefficient [-]
p_2	Outlet static pressure [Pa]	σ	Cavitation number [-]
Q	Flow rate [m^3/sec]	σ_B	Breakdown cavitation number [-]
Q_d	Design flow rate [m^3/sec]	ψ_{st} , ψ_s	Head coefficient based on static pressure [-]

References

[1] Tsujimoto, Y., Kamijo, K. and Brennen, C.E., 2001, “Unified Treatments of Instabilities of Turbomachines”, AIAA Journal of Propulsion and Power, Vol.117, No.3, pp.636-643.

[2] Young, W. E., 1972, “Study of Cavitating Inducer Instabilities”, Final Report, NACA-CR-123939.

[3] Shimura, T., Yoshida, M., Kamijo, K., Uchiumi, M. and Yasutomi, Y., 2002, “Cavitation Induced Vibration Caused by Rotating-stall-type Phenomenon in LH2 Turbopump”, Proc. of the 9th International Symposium on Transport Phenomena and Dynamics of Rotating Machinery, Honolulu, Hawaii, February 10-14.

[4] Semenov, Y., Fujii, A., Tsujimoto, Y., 2004, “ Rotating Choke in Cavitating Inducer”, ASME Journal of Fluids Engineering, Vol.126, No.1, pp.87-93.

[5] Uchiumi, M. and Kamijo, K., 2008, “Occurrence Range of a Rotating-stall-type Phenomenon in a High Head Liquid Hydrogen Inducer”, Proc. of the 12th International Symposium on Transport Phenomena and Dynamics of Rotating Machinery, Honolulu, Hawaii, February 17-22.

[6] Brennen, C. E. and Acosta, A. J., 1973, “Theoretical, quasistatic analysis of cavitation compliance in turbopumps”, J. of Spacecraft and Rockets, Vol.10, No.3, pp. 175-180.

[7] Yokota, K., Kurahara, K., Kataoka, D., Tsujimoto, Y. and Acosta, A., 1999, “A Study of Swirling Backflow and Vortex Structure at the Inlet of an Inducer”, JSME International Journal, Ser. B., Vol.142, No.3, pp.451-459.

[8] Furukawa, A., Ishizaka, K. and Watanabe, S., 2001, “Experimental Study of Cavitation Induced Oscillation in Helical Inducers with Various Blade Lengths”, Transactions of JSME (in Japanese), Ser. B, Vol.67, No.662, pp.37-42.

[9] Yoshida, Y., Seiji, A., Tsujimoto, Y. and Laffite, S., 2001, “Effects of Leading Edge Sweep on Unsteady Cavitation in Inducers (2nd report, Problems of Forward and Backward Sweep)”, Transactions of JSME, Ser. B, Vol.67, No.658, pp.1367-1375.

[10] Brennen, C. E., 1994, Hydrodynamics of Pumps, Concepts ETI, Inc. and Oxford University Press.